Non-Boussinesq and penetrative convection in a cylindrical cell

By R. W. WALDEN

Bell Laboratories, Murray Hill, NJ 07974

AND GUENTER AHLERS

Bell Laboratories, Murray Hill, NJ 07974 and
Department of Physics, University of California,
Santa Barbara, CA 93106

Measurements of Rayleigh numbers R and Nusselt numbers N have been made for a cylindrical cell having a radius to height ratio of 4·72 and containing liquid helium I. The upper surface of the cell was maintained at a constant temperature T_2 near $T_0 = 2·178$ K where the fluid density has a maximum. The heat input to the cell bottom was varied quasi-statically while the lower surface temperature T_1 was recorded. The penetration parameter $\mathscr{P} \equiv (T_1 - T_2)/(T_1 - T_0)$ ranged between 0·1 and 3 for our experiments.

For $\mathscr{P} < 1$, the initial slope of $N(R)$ for R near the critical Rayleigh number R_c was independent of $\mathscr{P}$. For $\mathscr{P} \gtrsim 1$, two hysteresis loops of $N(R)$ were observed. One of them occurred very near R_c and is interpreted in terms of the inverted bifurcation associated with the onset of cellular convection of non-Boussinesq systems. The other, for $R > R_c$, is believed to correspond to the transition from cellular to two-dimensional flow. Near R_c and with $\mathscr{P} > 2$ we also observed multistability, with the states believed to correspond to different numbers of convective cells.

For large $\mathscr{P}$ the onset of time-dependent flow occurred much closer to R_c than is the case for Boussinesq systems.

1. Introduction

Experimental studies of convection in fluid layers contained between horizontal parallel plates and heated from below have concentrated primarily upon systems which come close to satisfying the approximation of Oberbeck (1879) and of Boussinesq (1903) (OB). In that approximation, the temperature dependences of fluid properties are neglected, except for thermally induced density differences when they induce buoyant forces. Of those few experimental studies which were devoted to non-OB systems, the work of Somerscales & Dougherty (1970), Hoard, Robertson & Acrivos (1970), Richter (1978), Dubois, Berge & Wesfried (1978) and Ahlers (1980) are particularly notable; but these investigations either have been of a qualitative nature and have concentrated upon visual observations of convection flow patterns, or have been limited to a narrow range of the parameters which describe the departures from the OB approximation. In particular, there have been no systematic quantitative measurements of the two hysteresis loops associated with the inverted bifurcations near the

convection onset which are predicted to exist in non-OB systems (see, for instance, Busse 1967). The present paper covers a wide range of departures from the OB approximation, and includes a systematic study of the sizes and nature of the predicted hysteresis loops.

There have been several theoretical investigations of the effect of departures from the OB approximation (Palm 1960; Segel & Stuart 1962; Segel 1965; Palm, Ellingsen & Gjevic 1967; Busse 1967; Davis & Segel 1968). Of these, the work of Busse (1967) appears most complete in the sense that it considers the effect of temperature variations in *all* relevant fluid properties, and the effect of finite Prandtl numbers σ upon the problem. We will therefore compare our results primarily to the predictions of Busse.

The theoretical predictions for non-OB convection pertain to a system of infinite lateral extent. For that case, there should be a range near R_c where three-dimensional flow in the form of a hexagonal pattern is stable. Further above R_c, it is expected that two-dimensional flow in the form of straight rolls is stable. Clearly, this situation cannot pertain *in detail* to our experimental cell, which is of finite lateral extent and of cylindrical symmetry. We, therefore, cannot *a priori* expect a direct correspondence between the predictions of Busse (1967) and our experimental results. None the less, we find that our experimental data are described remarkably well by the predictions of Busse.

The working fluid used in our investigation was liquid ^{4}He at saturated vapour pressure and at temperatures above the super-fluid transition temperature

$$T_\lambda = 2{\cdot}1720 \text{ K}$$

where ^{4}He obeys the usual laws of classical hydrodynamics. We chose temperatures near $T_0 = 2{\cdot}178$ K where the liquid density has a maximum. By adjusting the temperature T_2 at the top of the fluid to a value close to but greater than T_0, the thermal expansion coefficient α_p was kept positive but varied considerably over the height of the fluid layer. Thus, in this investigation the source of departures from the OB approximation was primarily the temperature dependence of α_p. The extent Q (as defined by Busse 1967; see also Ahlers 1980) of departures from the OB approximation could be adjusted by varying T_2 in the range $T_2 \geqslant T_0$ (see figure 1) and covered the range from $Q = -0{\cdot}2$ for relatively high T_2 to $Q \cong -7$ for $T_2 \cong T_0$. It is for this range of parameters that we can expect the theory of Busse (which for laterally infinite systems is expected to be exact in the limit of small Q) to be applicable.

The experiments were extended further by permitting T_2 to be less than T_0 (see figure 1). In that case, the fluid near the top of the cell has $\alpha_p < 0$ and by itself would be stable in the gravitational field. Convection will, however, start in the unstable lower fraction of the cell where $\alpha_p > 0$, and the flow will tend to penetrate into the upper layer where $\alpha_p < 0$. Although this region of penetrative convection does not necessarily differ in a fundamental way from the non-OB convection considered by Busse (1967), we do not expect the predictions to be quantitatively applicable in the region of strong penetration because the expansion parameter Q of the theory becomes large. In fact, Q diverges when the static temperature T_{s0} at the mid-plane of the cell is equal to T_0. Thus, it is more convenient to discuss the extent of penetrative convection in terms of a different parameter, which we call $\mathscr{P}$, and which is essentially equal to the ratio of the cell height to the height of the unstable (lower) layer where $\alpha_p > 0$. Penetrative convection thus corresponds to $\mathscr{P} > 1$. Our investigation covers the
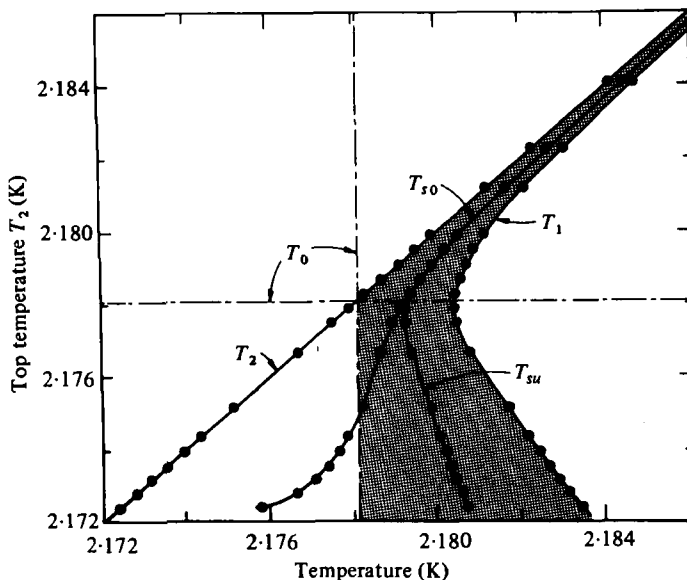
FIGURE 1. Experimental temperatures at the onset of convection. T_1 and T_2 are the temperatures at the bottom and top of the cell respectively. The thermal expansion coefficient vanishes for $T = T_0$. T_{s0} and T_{su} are the static temperatures at the horizontal midplane of the convection chamber and of the unstable fluid layer respectively (cf. figure 12 below). The shaded region denotes the unstable portion of the fluid layer before convection begins.

range up to $\mathscr{P} \simeq 3$. There have been several theoretical investigations of penetrative convection (Veronis 1962; Musman 1968; Moore & Weiss 1973; Merker, Waas & Grigubb 1979); but these theories either neglect the nonlinear terms altogether and thus predict only R_c, or assume boundary conditions at the top and bottom of the cell which are unrealistic for the experimental system. In addition, the calculations were done primarily for the case of water which has a Prandtl number an order of magnitude greater than our fluid. For these reasons a quantitative comparison with our results is not particularly fruitful, except for the critical Rayleigh number R_c, which is not as sensitive to some of the approximations in the theory.

The remainder of this paper is divided into the following sections. In §2 we will review very briefly the experiment. A detailed description of the apparatus will be given elsewhere (Behringer & Ahlers 1982, hereafter referred to as I). Section 3 summarizes briefly the theoretical predictions by Busse (1967) for moderately non-OB systems, and mentions previous experiments. A more detailed summary of the predictions is given by Ahlers (1980). In §4 we present our results for non-OB systems in the range of Q where we can reasonably expect the expansion in Q to be valid. We find that the initial dependence of N upon R above R_c is independent of Q within our resolution, consistent with the prediction. However, we find that our data for $R_c(Q)$ suggest a *linear* dependence $R_c = R_{c0}(1 - 0.005|Q|)$. The earlier data by Ahlers (1980) covered a narrower range of $|Q|$ and had more scatter, and were *consistent* with R_c independent of Q; but they too *suggest* a slight decrease of R_c with increasing $|Q|$. We had expected the theory (Busse 1967) to be correct to first order in Q, and thus had anticipated only terms of $O(Q^2)$ for $R_c(Q)$. We also present results for the sizes of the hysteretic transitions which occur near R_c between hexagonal (three-dimensional) flow, roll (two-dimensional)

4

flow, and the conducting state. The sizes of the measured hysteresis loops are remarkably consistent with Busse's (1967) prediction. In §5 we mention briefly various theoretical attempts to discuss penetrative convection, and previous experiments for this range of parameters. Section 6 contains our experimental results for penetrative convection ($|Q| \gtrsim 7$). In the range of strong penetration the theory of Busse (1967) is not quantitatively applicable; but we expect that the qualitative prediction of the existence of two hysteresis loops should remain valid. Indeed, we were able to resolve and measure the size of both hysteresis loops, even in the case of strong penetration. In the region of strong penetration we find multistability in the three-dimensional flow regime, and interpret it to correspond to different numbers of flow cells in our sample of finite lateral extent. In §7 we make some general remarks about our observations regarding time-dependent states observed during this work, and §8 summarizes our findings.

Some of the results presented in this paper have been reported briefly elsewhere (Walden & Ahlers 1979).

2. Apparatus and fluid properties

The apparatus will be described in detail in I. The working fluid for the measurements reported here was liquid ⁴He at vapour pressure. It was contained in a cylindrical cell (cell A of I) with a height $d = 0.2649 \pm 0.002$ cm and diameter $D = 2.502 \pm 0.002$ cm (aspect ratio $L \equiv D/2d$ equal to 4.72). The top and bottom boundaries were isothermal copper plates having a thermal relaxation time of 10^{-3} s. The walls were constructed of 0.013-cm-thick stainless steel. All heat conductivity measurements were corrected for wall heat conduction (see I).

The effective thermal conductivity λ_{eff} was determined by imposing a time-independent heat current q and measuring the temperature increase of the bottom plate while holding constant the temperature of the top plate. One can express λ_{eff} in terms of the Nusselt number $N \equiv \lambda_{\text{eff}}/\lambda$, where λ is the thermal conductivity of the fluid at rest. For the laterally infinite system N is a function of two dimensionless parameters, the Rayleigh number

$$R = g\alpha_p(T_1 - T_2)\,d^3/\kappa\nu \qquad (2.1)$$

and the Prandtl number

$$\sigma = \nu/\kappa. \qquad (2.2)$$

Here g is the gravitational acceleration, α_p the isobaric thermal expansion coefficient, ν the kinematic viscosity, κ the thermal diffusivity, and T_1 and T_2 are respectively the temperatures at the bottom and top of the cell. For the finite system, N depends also upon L (Charlson & Sani 1970; Behringer & Ahlers 1977; Ahlers *et al.* 1981). Parametrizations of the fluid properties used in our calculations are taken from I.

Liquid ⁴He at saturated vapour pressure has a density maximum a few millikelvins above the superfluid transition ($T_0 = 2.178$ K at $\alpha_p = 0$). Below the superfluid transition, heat transport occurs by superfluid counterflow such that $\nabla T = 0$ for moderate heat input, and classical convection does not occur. The range of experimental conditions which we explored is illustrated in figure 1. The Prandtl number σ is nearly constant and close to 0.78 in this range.

It is worth emphasizing that any spontaneous transitions from an unstable to a stable state will *not* follow a path of constant R (or ΔT) in our experiment because of

the constaint of constant q. Instead, the transitions will follow sloping lines in the N–R plane, such as those in figures 9 and 17 below.

3. Non-Boussinesq convection, predictions and previous experiments

Busse (1967) introduced the parameter

$$Q = \sum_{i=0}^{4} \gamma_i P_i \qquad (3.1)$$

to describe the extent of departures from the Oberbeck–Boussinesq approximation.†
Here

$$\gamma_0 = -(\rho_1 - \rho_2)/\rho, \quad \gamma_1 = (\alpha_{p1} - \alpha_{p2})/2\alpha_p,$$
$$\gamma_2 = (\nu_1 - \nu_2)/\nu, \quad \gamma_3 = (\kappa_1 - \kappa_2)/\kappa, \quad \gamma_4 = (C_{p1} - C_{p2})/C_p, \qquad (3.2)$$

where ρ is the density, and C_p the heat capacity at constant pressure. Fluid properties with subscripts 1 and 2 are to be evaluated for temperatures T_1 and T_2 at the lower and upper fluid boundaries respectively. The unsubscripted properties are evaluated at the static temperature T_{s0} at the horizontal midplane of the fluid layer. Values of P_i, which are functions of σ, are given by Busse (1967). Busse predicted that the critical Rayleigh number R_c and the initial dependence of the Nusselt number upon Rayleigh number for $R > R_c$ are not influenced to first order in Q by non-OB effects, provided R is evaluated at T_{s0}. Measurements by Ahlers (1980) over the range $0 < Q < 2$ are consistent with this prediction.

For an OB system, theory (e.g. Schlüter, Lortz & Busse 1965; Busse 1967) predicts and experiments (cf. Normand, Pomeau & Velarde 1977; Koschmieder & Pallas 1974; Koschmieder 1974) confirm that buoyancy-driven convection is initiated with a pattern of two-dimensional rolls at the critical Rayleigh number R_c. In that case, the instability occurs via a normal bifurcation. However, when departures from the OB conditions are introduced into the stability analysis (Busse 1967; Palm 1960; Segel & Stuart 1962; Segel 1965; Palm *et al.* 1967; Davis & Segel 1968), there is a finite range of Rayleigh numbers near the onset of convection for which the flow pattern consists of hexagonal cells. The instability at R_c then is an inverted bifurcation, and the flow evolves at R_c with a finite amplitude and in a hexagonal pattern. This is illustrated schematically in figure 2. With increasing R, the hexagons are stable for $R < R_b$, where $R_b > R_c$. With decreasing R, hexagons remain stable for $R > R_a$, where $R_a < R_c$. For $R < R_a$, the hexagons decay to the conducting state. For $R > R_b$, hexagons become unstable and finite-amplitude rolls will evolve. Upon decreasing R, the rolls remain stable for $R > R_r$, and there is a region of bistability between R_r and R_b. Values of R_a, R_r, and R_b have been calculated by Busse (1967) for a laterally infinite system and are given by

$$(R_a - R_c)/Q^2 = -R_H^{(20)}/4, \qquad (3.3a)$$

$$(R_b - R_c)/Q^2 = (9R_H^{(20)} - 3L_2)/L_2^2 \qquad (3.3b)$$

and

$$(R_r - R_c)/Q^2 = 3R_H^{(20)}/L_2^2, \qquad (3.3c)$$

where $R_H^{(20)}$, $R_R^{(20)}$, and L_2 are weak functions of the Prandtl number. Appropriate values for our experiments were obtained from Busse (1967) by Ahlers (1980).
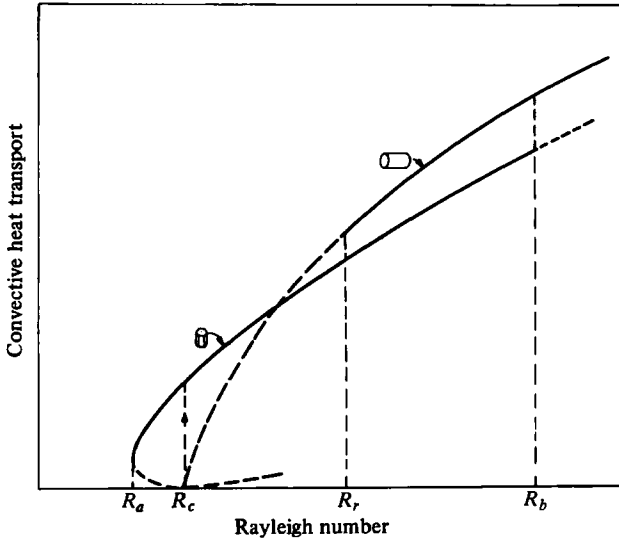
† Our parameter Q is the same as Busse's (1967) P.

FIGURE 2. Schematic illustration of the hysteretic transitions between pure conduction and two-dimensional and three-dimensional convective heat transport (see text). The drawing is exaggerated for clarity – typically $(R_c - R_a):(R_r - R_c):(R_b - R_c) = 1:25:100$ in the range of our experiments.

Several visual experiments (Silveston 1958; Koschmieder 1966; Somerscales & Dougherty 1970; Hoard et al. 1970) in cylinderical test chambers with high-Prandtl-number fluids have tended to confirm qualitatively these predictions, except that hysteresis between R_a and R_c was not observed. However, it appears that variations in the thermal and physical boundary conditions and the rate of temperature change in some of these experiments significantly affected the observed flow evolution. Somerscales & Dougherty (1970) reported circular rolls at the onset of convection for small Q; but for $Q > 1.5$ the initial flow was in the form of hexagonal cells. Krishna-murti (1968) showed that changing the mean fluid temperature at a constant rate, and thus introducing a nonlinearity into the conductive temperature profile, also produced a flow pattern of hexagons near R_c, whereas with constant mean temperature two-dimensional rolls appeared at the onset of convective flow.

Richter (1978) has studied the effect of strong variations in the viscosity on convection in containers of large lateral extent. He finds flow in the form of hexagons immediately above R_c, but has not studied quantitatively the range of existence of this three-dimensional flow state.

Dubois et al. (1978) have reported local measurements of the fluid velocity in a water layer whose top temperature is maintained constant near the density maximum at 4 °C. Convection is initiated at R_c with a jump to finite flow velocity in a pattern of hexagonal cells. Increasing R, then decreasing R again to R_c carries the system through a hysteresis loop between hexagons and rolls, qualitatively like that illustrated in figure 2 between R_r and R_b. However, Dubois et al. did not have sufficient resolution to observe the expected hysteresis between onset of convection at R_c and its cessation at $R_a < R_c$.

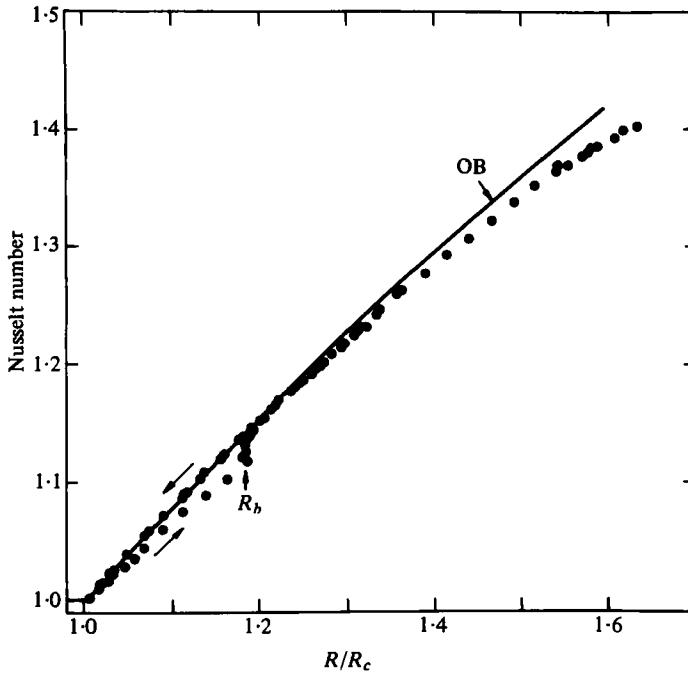An interesting recent study using water between 0 °C and 4 °C has been reported

FIGURE 3. Nusselt number as a function of the reduced Rayleigh number R/R_c. $Q_c = -3.77$, $\mathscr{P} = 0.75$. Hysteresis between three-dimensional convection (lower branch) and two-dimensional rolls (upper branch) is observed.

by Azouni & Normand (1981); but this work was for aspect ratios of order unity and less, and the qualitative behaviour of the system was determined by the boundaries. This work therefore makes relatively little contact with our own results.

4. Results for non-Boussinesq convection

In this section we present those of our results which can reasonably be expected to fall into the range of applicability of the predictions by Busse (1967). That range apparently corresponds to $Q^2 \leqslant R_c$ (Ahlers 1980), and thus $|Q| \leqslant 40$ ($R_c = 1708$ for the laterally infinite system). We would therefore expect the entire range of non-penetrative convection (i.e. $\alpha_p \geqslant 0$ throughout the cell), which has $|Q| \leqslant 6.63$, to be suitable for comparison with the theory. We will, however, present some results also for larger $|Q|$, keeping in mind that deviations from the theory may occur as $|Q|$ grows.

For all data reported in this section, Rayleigh numbers were evaluated at the static temperature T_{s0} at the horizontal mid-plane of the cell (Busse 1967; Ahlers 1980).

The general features for non-penetrative convection are illustrated by the results shown in figure 3. A hysteretic transition, presumed to be between three-dimensional and two-di mensional convection flow,† is resolved for $|Q_c| \gtrsim 2$ (Q_c is the value of Q when $R = R_c$). The upper limit of the hysteresis loop occurs at a value of $\bar{\epsilon} \equiv R/R_c - 1$ which we associate with R_b (figure 2), and which grows with increasing $|Q|$

† Although we have no visual observations of the flow geometry, we shall refer to the two states evident from figure 3 as hexagonal and roll flow.
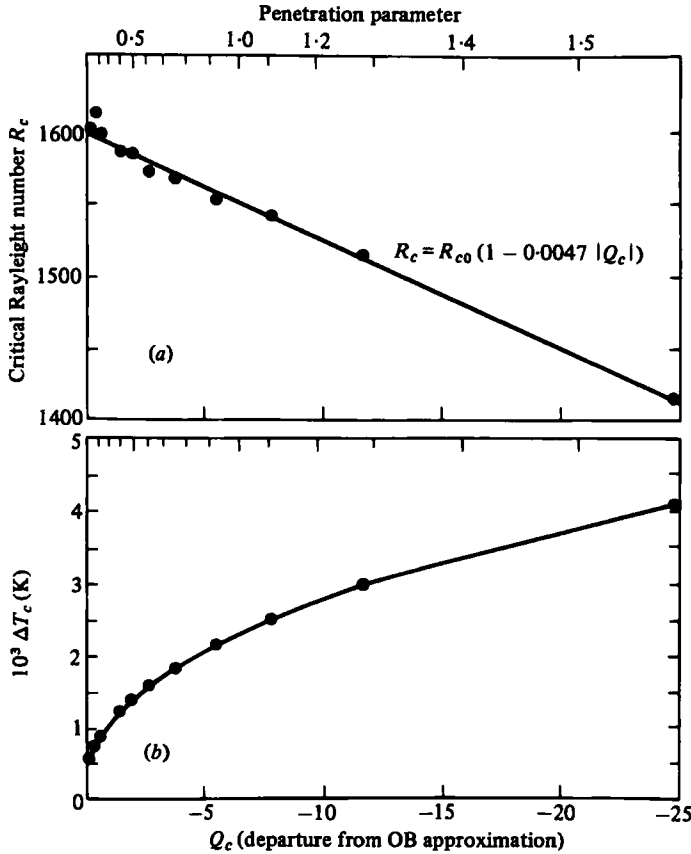
FIGURE 4. (a) Critical Rayleigh numbers R_c as a function of Q_c. The value of Q_c is a measure of the extent of departures from the Oberbeck–Boussinesq approximation. (b) Critical temperature difference ΔT_c as a function of Q_c.

approximately as Q^2, as expected from (3.3b). We will now discuss the critical Rayleigh numbers, the initial slope of the Nusselt numbers, and the sizes of the hysteresis loops.

For our finite OB systems, we expect a bifurcation from the conducting to the convecting state at

$$R_{c0} = R_{c0}^\infty (1 + \epsilon_c),\qquad (4.1)$$

where ϵ_c depends upon L (Charlson & Sani 1970; Brown & Stewartson 1978; Ahlers *et al.* 1981). The results for $R_c(Q_c)$ with $|Q_c| \leqslant 25$ are collected in figure 4a, and should extrapolate to R_{c0} at $Q = 0$. The corresponding values of the temperature difference ΔT_c when $R = R_c$ are shown in figure 4(b). Within our resolution, R_c can be described by a *linear* function of Q_c, as illustrated by the solid line in figure 4(a). In the limit of vanishing Q_c, the data yield $R_{c0} = 1600$; but this value is subject to considerable systematic errors due to systematic uncertainties in the fluid properties and in the height of the convection cell. A comparison with the theoretical estimates is given in **I**.

The finite slope of $R_c(Q_c)$ near $Q_c = 0$ is contrary to the theoretical prediction for the laterally infinite system (Busse 1967) which implies deviation of R_c from R_{c0} to be of $O(Q^2)$. Of course, we do not know whether a theory for the finite system might
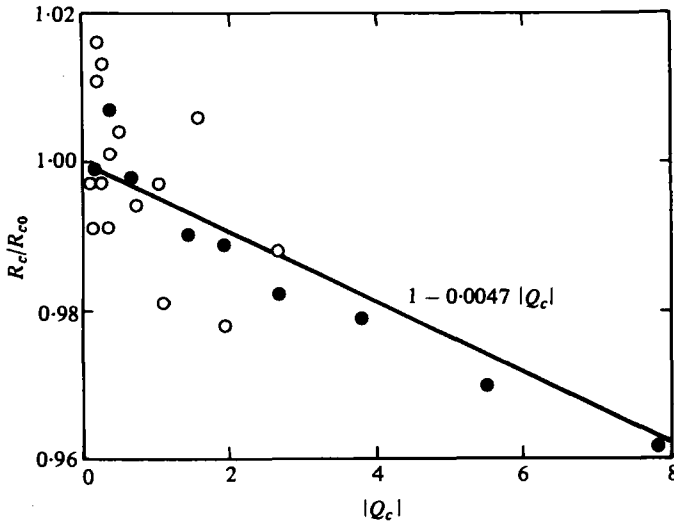
FIGURE 5. Critical Rayleigh numbers R_c, normalized by the value of R_c for Boussinesq systems, as a function of Q_c. $\bigcirc$, Ahlers 1980; $\bullet$, this work.

yield terms of $O(Q)$. On the experimental side, we are unable to determine with absolute certainty that temperature-dependent systematic errors in the fluid properties used to obtain $R_c(Q_c)$ are sufficiently small to rule out an R_c independent of Q_c. As an example of the sensitivity of $R_c(Q_c)$ to the details of the data analysis we mention that the slope of $R_c(Q_c)$ increases by a factor of 3 if the fluid properties at $\frac{1}{2}(T_1 + T_2)$ are used instead of at T_{s0}.

The earlier results of Ahlers (1980) had not revealed a Q-dependence of R_c. In order to compare our data with them, we show in figure 5 R_c/R_{c0} on an expanded vertical scale for $|Q_c| \leqslant 8$. The normalization by R_{c0} largely eliminates different systematic errors for the two data sets from the comparison. The earlier data have more scatter and do not by themselves establish a Q-dependence of R_c; but they are consistent with the Q-dependence shown by the solid line in figure 5 and tend to support a mildly Q-dependent R_c.

The solid line in figure 3, labelled OB, represents a least-squares fit over the range $1 \cdot 008 \leqslant R/R_c \leqslant 1 \cdot 11$ to data for $Q_c = -0 \cdot 19$ from I. In spite of the inverted bifurcations near R_c, the initial $\bar{\varepsilon}$-dependence of N for the rolls is unaltered within experimental resolution by the non-OB character of the sample. This is demonstrated in more detail in figure 6, where we show $(N-1)/\bar{\varepsilon}$ for three values of Q_c. For the purpose of this figure, $\bar{\varepsilon}$ was based on values of R_c derived from least-squares fits to the roll data. We see that $(N-1)/\bar{\varepsilon}$ is nearly constant and independent of Q_c for Q_c as large as -4 for both hexagons and rolls. Ahlers (1980) reported similar observations for rolls and positive Q_c up to 2. The absence of a Q-dependence of the initial slope of $N(R)$ for the rolls agrees with the prediction of Busse (1967) for the infinite system. For the hexagons, the theory for the infinite system predicts that $(N-1)/\bar{\varepsilon}$ should diverge at $\bar{\varepsilon} = 0$ because $N-1$ is non-zero (see figure 2). This is illustrated in figure 7, where the predicted convective heat transport $(N-1) R/R_c$, divided by ε, is shown as a function of R/R_c. The solid line is for rolls, except that the parameter $R_H^{(20)}$ of Busse (1967) was changed from the theoretical value to fit the experimental values of $N(R)$. The dashed
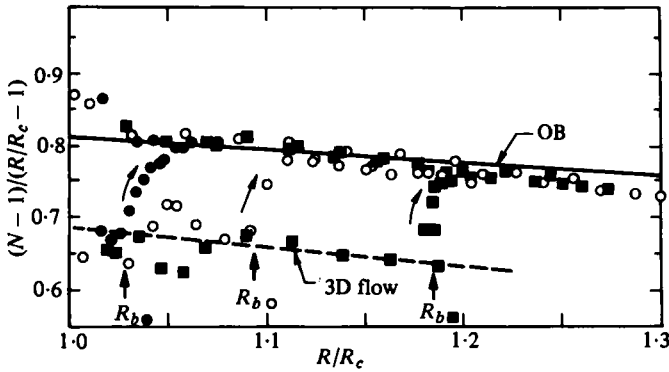
FIGURE 6. The 'slope' of $N(R/R_c)$ as a function of reduced Rayleigh number R/R_c for three values of Q_c. The value of Q_c is a measure of the extent of departures from the Oberbeck-Boussinesq approximation; $\mathscr{P}$ is the penetration parameter. Transitions from three-dimensional to two-dimensional convective patterns are identified as R_b. $\bullet$, ($Q_c = -1.96$, $\mathscr{P} = 0.50$); $\bigcirc$, $(-2.68, 0.62)$; $\blacksquare$, $(-3.77, 0.75)$.
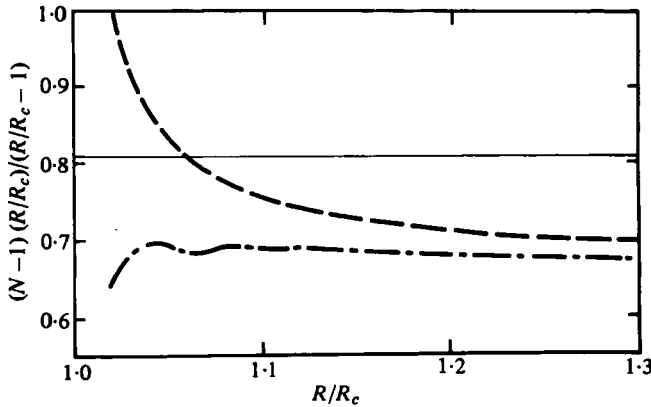

FIGURE 7. Theoretical prediction for $(N-1)(R/R_c)/(R/R_c-1)$ for rolls (solid line) and hexagons (dashed line). $Q_c = -3.77$. Parameters in the theory were adjusted to fit the data in figure 6 at large R/R_c. The shape of the dashed line is inconsistent with the hexagon data in figure 6. Consistency can be obtained by a small shift in R_c for hexagons relative to R_c for rolls, as illustrated by the dash-dotted line.

line is the prediction for hexagons with $Q = -3.77$, but with $R_H^{(20)}$ of Busse (1967) adjusted to fit the experimental values of $N(R)$ at large R. Clearly, the data for hexagons with $Q_c = -3.77$ in figure 6 do not agree with the dashed line. However, we can bring the prediction into agreement with the data by assuming slightly different shifts, by increments ϵ_{cR} and ϵ_{cH}, of R_c from R_c^∞ for rolls and hexagons respectively. In particular, by assuming $\epsilon_{cH} - \epsilon_{cR} = 0.01$, we obtained the dash-dotted line in figure 7. That line is consistent with the hexagon data for $Q_c = -3.77$ in figure 6.

In order to present our results in a more quantitative way, we fitted the data for the rolls over the appropriate range (see Ahlers 1980) to the equation

$$N - 1 = \sum_{i=1}^{n} N_i \bar{\epsilon}^i.$$

Here $\bar{\epsilon} \equiv R/R_c - 1$. Both R_c and the N_i were adjusted. The results are summarized in

T_s (K)	ΔT_c (μK)	Q_c	R_c (n = 2)	$S = (dN/dR)_c$		$\mathscr{P}_c$
				(n = 1)	(n = 2)	
2·18409	600	−0·19	1599	0·77	0·82	0·091
2·18224	762	−0·39	1611	0·82	0·84	0·155
2·18117	911	−0·65	1597	0·81	0·78	0·228
2·17987	1240	−1·46	1584	0·81	0·87	0·411
2·17948	1398	−1·96	1583	0·80	0·78	0·502
2·17908	1589	−2·68	1571	0·71	0·86	0·616
2·17869	1837	−3·77	1566	0·66	0·84	0·755
2·17828	2156	−5·50	1552	0·60	0·80	0·921
2·17790	2516	−7·83	1540	—	—	1·103
2·17749	2989	−11·68	1514	0·40	0·76	1·286
2·17670	4080	−24·78	1415	—	—	1·575

TABLE 1. Experimental conditions and derived parameters.
The penetration parameter $\mathscr{P}$ is defined in the text.

T_s (K)	ΔT_c (μK)	$\mathscr{P}_c$	$\bar{\epsilon}_{aT}$	$\bar{\epsilon}_a$
2·17790	2516	1·103	0·0016	0·0037
2·17749	2989	1·286	0·0049	0·0125
2·17670	4080	1·575	0·0106	0·044
2·17515	6566	1·949	0·0113	
2·17436	7829	2·111	0·0097	
2·17397	8453	2·198	0·0097	
2·17358	9085	2·294	0·0084	
2·17318	9703	2·417	0·0070	
2·17279	10352	2·582	0·0062	
2·17240	11025	2·874	0·0049	

TABLE 2. Amplitude of hysteresis at the onset of convection.

table 1 for $n = 1$ and 2 (larger n gave parameters similar to $n = 2$). Even for $|Q_c| > 10$, in which case rolls are observed only outside the range of figure 6, the slope determined from the roll data and with $n = 2$ differs by only about 6 % from the OB value.

Schlüter *et al.* (1965) have calculated the values of the initial slopes for the laterally infinite system. For $\sigma = 0.78$ the predicted slopes are 1·414 for straight rolls and 0·936 for hexagons. The experimental results, from figure 6, are 0·82 and 0·69 respectively. They are smaller than the theoretical results because of the cylindrical boundaries of the experimental cell (Behringer & Ahlers 1977; Ahlers 1980; Ahlers *et al.* 1981). Although the depression of N_1 below the value of the laterally infinite system is readily understood in terms of the boundaries, one might have expected the *ratio* of the initial slopes for rolls and hexagons to be nearly unaltered by the lateral boundaries of the system (Ahlers *et al.* 1981). For the infinite system, the theoretical ratio is 1·47, whereas the experiment yields the considerably smaller value 1·17. We do not have a firm explanation for this, but consider it possible that the small experimental ratio is due to differences in the boundary conditions at the convection chamber centre for hexagons and rolls (see Ahlers *et al.* 1981).

As a last topic in this section, we turn to our results for the sizes of the hysteresis loops. Figures 3 and 6 illustrate our observation of $\bar{\epsilon}_b \equiv (R_b - R_c)/R_c$ (for the purpose
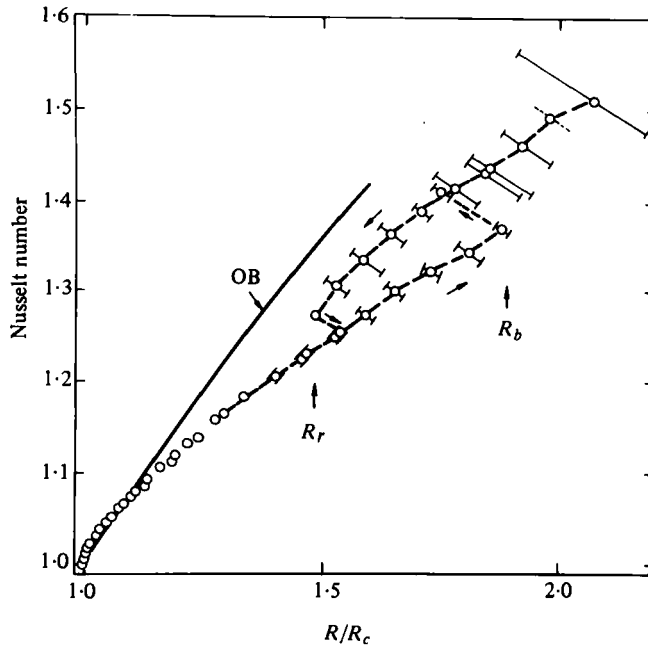
FIGURE 8. Nusselt number as a function of reduced Rayleigh number R/R_c. $Q_c = -11.68$, $\mathscr{P} = 1.29$. The diagonal bars indicate the range of excursions for time-dependent convection.

of those data the suggested 1 % difference in R_c for hexagons and rolls is insignificant). It is evident from figure 3 that the hexagon and roll data come rather close to each other as $\bar{\varepsilon}$ decreases and that it is not possible to observe the transition at R_r for that reason in this range of Q. For larger Q, we could resolve both R_r and R_b. This is shown in figure 8 for $Q_c = -11.68$. The very tiny hysteresis loop between R_a and R_c could be resolved in our measurements only for $|Q_c| \geqslant 7.8$, that is only in the region of penetrative convection. A number of examples are illustrated in figure 9. All the data for $\bar{\varepsilon}_b$, $\bar{\varepsilon}_r$, and $\bar{\varepsilon}_a$ with $|Q_c| \leqslant 28$ are collected in figure 10. The solid lines in this figure correspond to the predictions (3.3a)–(3.3c) for the laterally infinite system. For $\bar{\varepsilon}_b$, most of the experimental points are only about 10 % lower than the theoretical values. The result at the highest $|Q_c|$ ($Q_c = -11.68$) has $\bar{\varepsilon}_b$ nearly equal to 1, and may well be low compared with the theory because both Q_c and $\bar{\varepsilon}$ must be sufficiently small for the theory to apply. On the other hand, it is possible for the experiment to yield low results because a finite-amplitude experimental perturbation can cause a transition from hexagons to rolls in a range of $\bar{\varepsilon} < \bar{\varepsilon}_b$. This is illustrated by the two points in figure 10 at $Q_c = -5.5$. The data which resulted in those values of $\bar{\varepsilon}_b$ are shown in figure 11. In that case, *three* distinct states, labelled (a), (b), and (c), were revealed by the measurements. Transitions from (a) to (c) were observed, during separate experimental runs, at the values of R/R_c indicated by t_1 and t_2 in the figure. The corresponding values of $\bar{\varepsilon}_b$ are shown in figure 10. The transition at t_2 agrees well with the theoretical curve, and presumably is close to the upper limit of the stability range of hexagons. The transition at t_1 was premature, and we presume that it was caused by a finite-amplitude perturbation of unknown experimental origin.

The state (a) in figure 11 could always be obtained by slowly increasing the heat

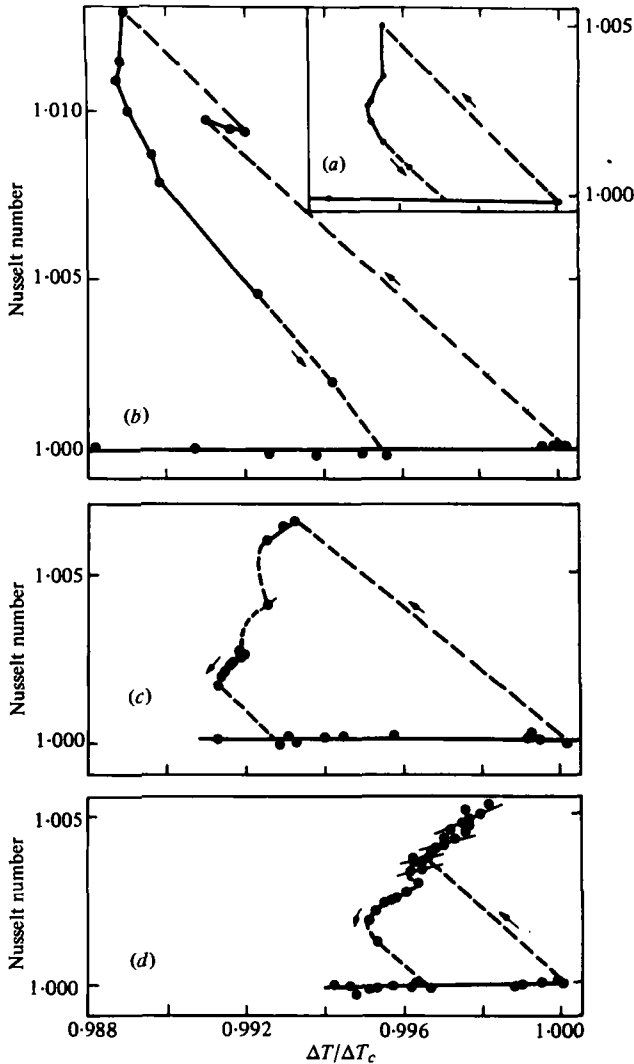FIGURE 9. Hysteresis loops at the onset of convection. Nusselt numbers as a function of reduced temperature differences $\Delta T/\Delta T_c$. (a) $\mathscr{P} = 1\cdot29$. (b) $\mathscr{P} = 1\cdot95$. (c) $\mathscr{P} = 2\cdot29$. (d) $\mathscr{P} = 2\cdot87$.

current q (over a period of many hours) from below to above the critical heat current q_c for onset of convection. The state (b) was created by a discontinuous jump in q from $q < q_c$ to $q \simeq 1\cdot3q_c$. We believe that state (b) corresponds to a three-dimensional flow, but with a characteristic wave vector different from that for state (a). State (b) also decayed to state (c), and the $N(R)$ data for state (c) are consistent with the roll data at other values of Q_c. The transition from (b) to (c) occurred at t_3, corresponding to a value of $\bar{\epsilon}_b$ greater than the point shown in figure 10.

For $\bar{\epsilon}_r$, we obtained only one value, corresponding to $Q_c = -11\cdot68$ and the data in figure 8. For smaller Q_c, we were unable to observe the transition because the associated jump in N was too small, and for more highly penetrative systems (figure 13 below) Q_c is no longer a meaningful parameter. The one point in the range of interest, shown as a solid circle in figure 10, is only 18 % smaller than the theoretical value.
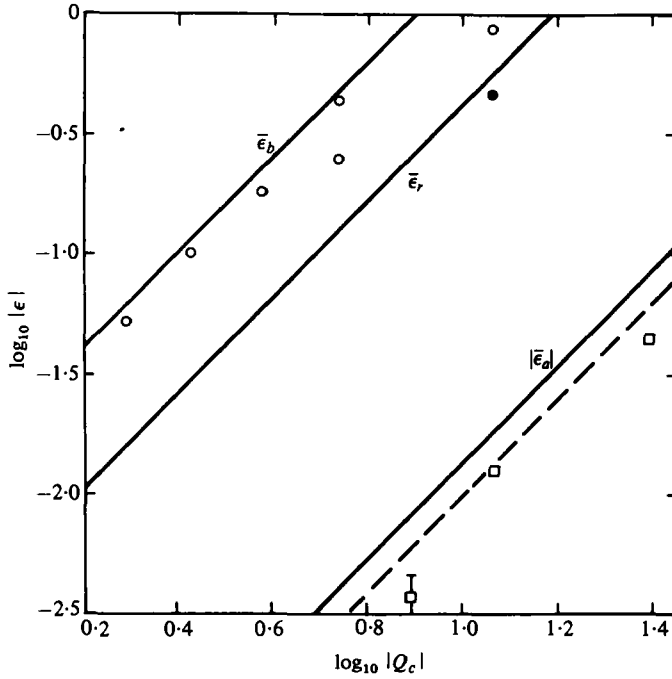
FIGURE 10. Values of $\bar{\epsilon} = R/R_c - 1$ at the hysteretic transition points R_a, R_r, and R_b (see figure 2), as a function of Q_c on logarithmic scales. The symbols are experimental data, and the solid lines are theoretical results from Busse (1967). The dashed line is the prediction for $\bar{\epsilon}_a$, with a parameter in the theory adjusted so as to fit the experimental $N(R)$ of our finite system.
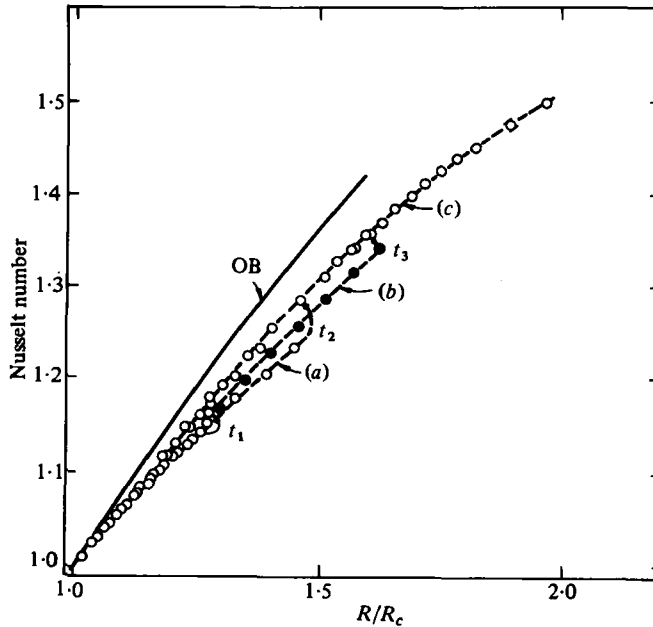

FIGURE 11. Nusselt number as a function of reduced Rayleigh number R/R_c. $Q_o = -5.50$, $\mathscr{P} = 0.92$. Transitions from convective states (a) and (b) to state (c) are identified by t_1, t_2 and t_3.

Measurements of $\bar{\epsilon}_a$ were very difficult because of the extremely small size of this hysteresis loop and the very long equilibration time near R_c. The result obtained at $Q_c = -7.83$ corresponds to a change in temperature difference of only about $4\,\mu\text{K}$, or $0.16\,\%$ of ΔT_c. For this point we show error bars in figure 10 corresponding to an uncertainty of about $\pm 1\,\mu\text{K}$. This uncertainty is due to long-term experimental drifts caused by the extremely slow process (of order one week to complete the hysteresis loop once) of taking equilibrium data so close to R_c. Generally, the data for $\bar{\epsilon}_a$ are somewhat lower (by about a factor of 2) than the prediction for the infinite system. We believe that this difference may be in part attributable to our lateral boundaries. It is interesting to note from (3.3) that $\bar{\epsilon}_a$ depends only upon $R_H^{(20)}$, whereas $\bar{\epsilon}_b$ and $\bar{\epsilon}_r$ involve also the experimentally unknown parameter L_2. We used our experimental value of the slope of $N(R)$ for hexagons (figure 6) to estimate $R_H^{(20)}$ for the finite system, and calculated $\bar{\epsilon}_a$ from (3.3a) with this experimental $R_H^{(20)}$. The result is the dashed line in figure 10, and is in much better agreement with the data. Of course, we consider this procedure to be only a very crude estimate of the effect of lateral boundaries. A comparison with a calculation for a finite system would be most interesting.

5. Penetrative convection: parameters, predictions and previous experiments

In the case of penetrative convection, for which $\alpha_p < 0$ in a fraction of the fluid, it is customary† to modify the definition of the Rayleigh number so that it refers only to the unstable fluid layer below the density maximum, i.e.

$$R_u = g\alpha_p \Delta T l^3 / \kappa\nu, \tag{5.1}$$

where, in the absence of convection, l is the depth of the *unstable* fluid layer,

$$\Delta T = T_1 - T_0$$

is the temperature difference across the *unstable* fluid layer, and α_p, κ and ν are determined at the static temperature of the mid-plane of the *unstable* layer.

Following Veronis (1962), we use the parameter $\mathscr{P} \simeq d/l$ ($\mathscr{P} \geqslant 1$) as a measure of the extent of the penetration. If the thermal conductivity is temperature independent, this is equivalent to

$$\mathscr{P} = (T_1 - T_2)/(T_1 - T_0), \tag{5.2}$$

and for convenience we extend the definition of $\mathscr{P}$ into the range $\mathscr{P} < 1$ by using (5.2).

Once convection begins, the convective flow penetrates well into the stably stratified layer. We may understand this qualitatively by reference to figure 12. Before convection is initiated the fluid layer between temperatures T_0 and some $T' < T_0$ (defined such that $\rho(T') = \rho(T_1)$) has a higher density than the fluid at temperature T_1 at the bottom of the container. Thus, when convective mixing is initiated,

---

† Several definitions of the Rayleigh number appropriate for penetrative convection have been suggested. For example, Sun, Chi & Yen (1969) proposed a rather complicated definition of R, based on a parametrization of the fluid density with a third-order polynomial. In this form they are able to predict and experimentally verify R_c for the ice–water system over a range of penetration parameters. However, there appears to be no advantage to the use of their definition *after* the onset of convection. Definitions of R which seem most appropriate once convection has begun depend on empirical determinations of the depth of the convecting layer (e.g. Moore & Weiss 1973; Musman 1968) which changes very rapidly with heat input q for ΔT near ΔT_c.
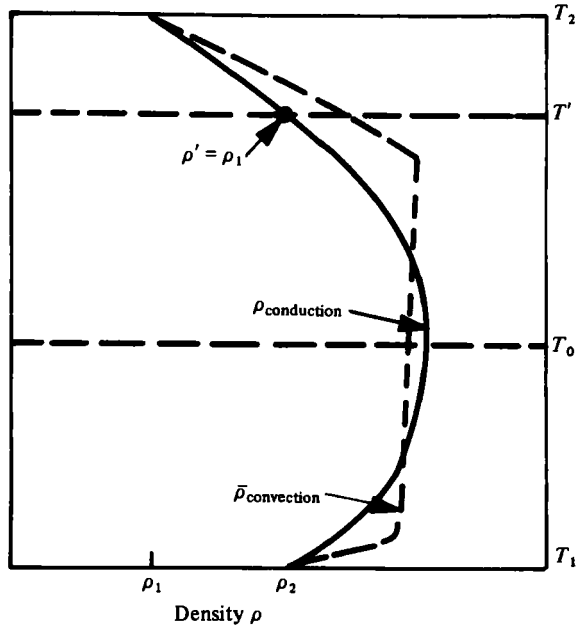
FIGURE 12. Vertical profiles of mean fluid density ρ in the static case
(conduction only) and with penetrative convection.

this global instability manifests itself by deep penetration of the convective flow into the locally stable layer between T_0 and T'. Dissipation due to viscous and thermal diffusion seems to limit penetration to somewhat less than the thickness of this layer (see, for example, Moore & Weiss 1973). At larger Rayleigh numbers turbulent convective mixing maintains the horizontally averaged temperature nearly constant over a significant fraction of the fluid height, while a large temperature gradient spans the narrow conduction layer at the top of the fluid (Furumoto & Rooth 1961; Adrian 1975; Myrup et al. 1970; Townsend 1964; Deardorff, Willis & Lilly 1969).

By extension of the theory relevant to moderate $Q(\mathscr{P} < 1)$ it is expected that penetrative convection will be initiated with three-dimensional flow for which there is hysteresis in the Rayleigh number at R_c. The ice–water experiments of Dubois et al. (1978) correspond to $\mathscr{P} = 1$. They do find three-dimensional convection, but without sufficient resolution near R_c to observe the hysteresis. Yen (1968) reported experiments in a cylindrical container initially filled with ice and heated from below. When sufficient ice had melted for penetrative convection to begin, a rectangular array of hemispherical depressions formed in the surface of the ice. With increasing convection these depressions grew in diameter and became irregular in shape. When this experiment was inverted so that melting ice formed the lower fluid boundary (Yen & Galea 1969), a concentric pattern of uniformly spaced rings first formed in the ice, followed by the appearance of the hemispherical cells. Tankin & Farhadieh (1971) reported experiments with ice and water in a rectangular cell for which they observed two-dimensional rolls at the onset of convection; however, it appears that thermal boundary conditions at the walls influenced their results, and again there was no indication of hysteresis at R_c.

Preliminary measurements similar to ours on penetrative convection using liquid helium have been reported by Ahlers (1975). Those results were obtained, however, with a cell of less uniform height than the present one. For that reason, $N(R)$ near R_c was appreciably rounded. This rounding prevented the observation of the hysteretic transitions near R_c.†

Theoretical models of penetrative convection (in ice and water) (Veronis 1963; Musman 1968; Moore & Weiss 1973) also predict a finite-amplitude instability below R_c, implying hysteresis in R at onset of convection; however, these models are not suitable for quantitative comparison with the experiments to be reported here. Musman and Moore & Weiss treat only the case of free–free boundary conditions and convective transport in a pattern of two-dimensional rolls, while the calculations of Veronis (which do consider the case of rigid boundaries and hexagonal convection cells) would need to be extended to higher order to permit quantitative comparison.

6. Results for penetrative convection

In this section we present the results of our measurements in the range $|Q| > 6\cdot63$ where $\alpha_p < 0$ in a fraction of the cell. The parameter Q is not very suitable to describe the extent of penetrative convection because $|Q|$ diverges when $\alpha_p = 0$ in the mid-plane of the cell. In that case, R as defined by (2.1) and evaluated at T_{s0} vanishes and likewise is not a meaningful parameter. We shall therefore express our results in terms of R_u (equation (5.1)) and $\mathscr{P}$ (equation (5.2)). In addition, we shall use also the primary measured parameter $\Delta T / \Delta T_c$ because the definition (5.1) of R_u may turn out to be inconvenient from the viewpoint of future theoretical developments.

We have already presented some results for mildly penetrative convection in §4 (see figures 8–10). Nusselt-number measurements in the range of strong penetration are illustrated in figure 13 for $\mathscr{P} = 2\cdot29$ as a function of $\Delta T / \Delta T_c$. The insert in the figure shows the same data as a function of $(R/R_c)_u$.

In figure 14 we show results for the critical value R_{cu} of the Rayleigh number R_u defined by (5.1). We have normalized R_{cu} to unity at $\mathscr{P} = 1$ (for $\mathscr{P} = 1$, R_u and R as given by (5.1) and (2.1) became identical) by dividing by $R_c(\mathscr{P} = 1) = 1550$ (see figure 4a) because our absolute Rayleigh numbers are not very accurate. Similarly-normalized calculations by Veronis (1962) are shown by the solid line. Those theoretical results are based upon a linear theory. They agree with the data for $\mathscr{P} \lesssim 1\cdot8$, and are somewhat high for larger $\mathscr{P}$. Theoretical results based on a nonlinear calculation (Musman 1968) are available only for free–free boundary conditions and cannot be compared directly with our data. But, for free–free boundaries, the nonlinear calculation of R_c lies below the linear calculation, suggesting that a nonlinear theory with rigid–rigid boundaries would lead to improved agreement with the data in figure 14 for $\mathscr{P} > 1\cdot8$.

In the range of strong penetration, we have not explored R_r and R_b as extensively as R_a, primarily because time-dependent behaviour of the fluid flow (see §7 below) made these measurements difficult and possibly unreliable. The example shown in figure 13, obtained in a range of $\mathscr{P}$ where the flow was relatively steady, suggests that

† The data of Ahlers (1975) revealed an increase with increasing $\mathscr{P}$ of the initial slope of $N(\Delta T / \Delta T_c)$. It was not realized at the time that $N(R/R_c)$, with R determined at T_{s0}, remained independent of $\mathscr{P}$ for R near R_c. The interpretation of those data in terms of a tricritical point is erroneous and should be disregarded.
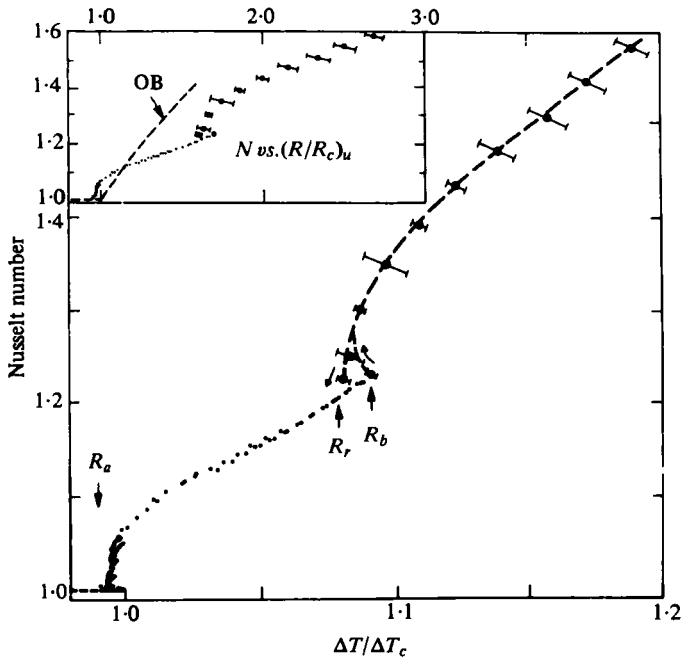
FIGURE 13. Nusselt number as a function of reduced temperature difference $\Delta T/\Delta T_c$. $\mathscr{P} = 2\cdot29$. Near $N = 1$ closely spaced data points are plotted as small dots to reveal some of the structure of the flow evolution. The tiny hysteresis loop at the onset of convection is shown greatly expanded in figure 9 (c). Since the usual Rayleigh number is meaningless for $\mathscr{P} > 2$, Nusselt numbers as a function of reduced Rayleigh number $(R/R_c)_u$ based on the unstable fluid layer are shown in the inset. The diagonal bars indicate the range of excursions for time-dependent convection.

the size of the hysteresis loop between R_r and R_b becomes relatively small at large $\mathscr{P}$.

Examples of our detailed measurements of the hysteresis loop between R_a and R_c have already been shown in figure 9. In figure 15 we give all our results for the size of this loop as a function of $\mathscr{P}$. That size is expressed in three different ways. The definition $\bar{\epsilon}_a = 1 - R_a/R_c$ was used already in figure 10, and is meaningful only to the left of the vertical line at $\mathscr{P} = 2$ in figure 15 because R (equation (2)) vanishes there. Results for $\bar{\epsilon}_a(\mathscr{P})$ are shown as solid circles. We also show the results of our measurements in terms of $\bar{\epsilon}_{au} = (1 - R_a/R_c)_u$, i.e. in terms of parameters evaluated for the unstable layer only. Those are the open circles in the figure. Finally, we also give as solid squares $\bar{\epsilon}_{aT} = 1 - \Delta T_a/\Delta T_c$, which relates most closely to the primary measured quantities.

For large penetration ($\mathscr{P} \gtrsim 2$), quasi-static changes in the heat current q for ΔT near ΔT_c resulted in a series of hysteretic but reproducible transitions closely spaced in ΔT: figure 16 shows an example. Those data correspond to the conduction state, and the three-dimensional flow state between R_a and R_c (see figure 2). They start on the left of the figure in the conducting state, but very close to ΔT_c. A small step in q yields $\Delta T > \Delta T_c$. Pure conduction is unstable there and the convecting hexagon state forms, accompanied by the dramatic drop in ΔT. The knee at A in the figure suggests the existence of an intermediate state. Similar effects have been observed at higher $\mathscr{P}$, sometimes with more than one knee. It is often possible to find a stable
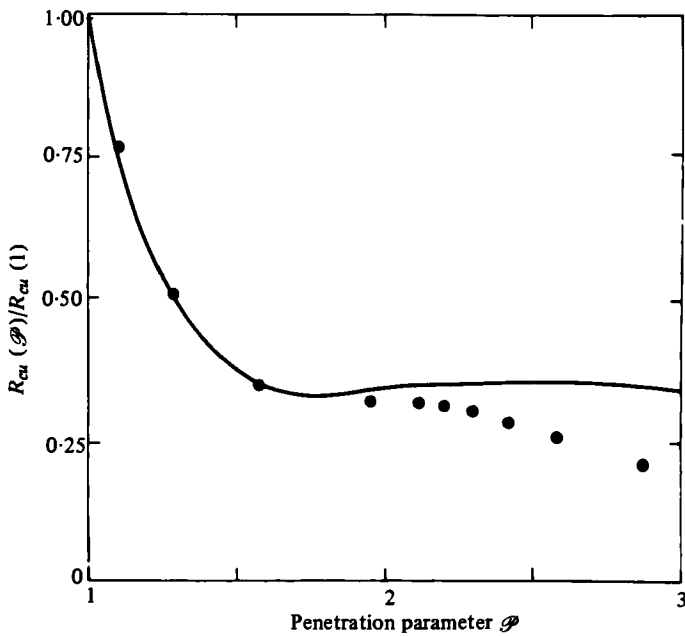
FIGURE 14. Critical Rayleigh numbers R_{cu} as a function of penetration parameter $\mathscr{P}$. The solid line is based on the linear theory of Veronis (1963); the values of R_{cu} were normalized by $R_{cu}(\mathscr{P} = 1)$ to facilitate comparison.
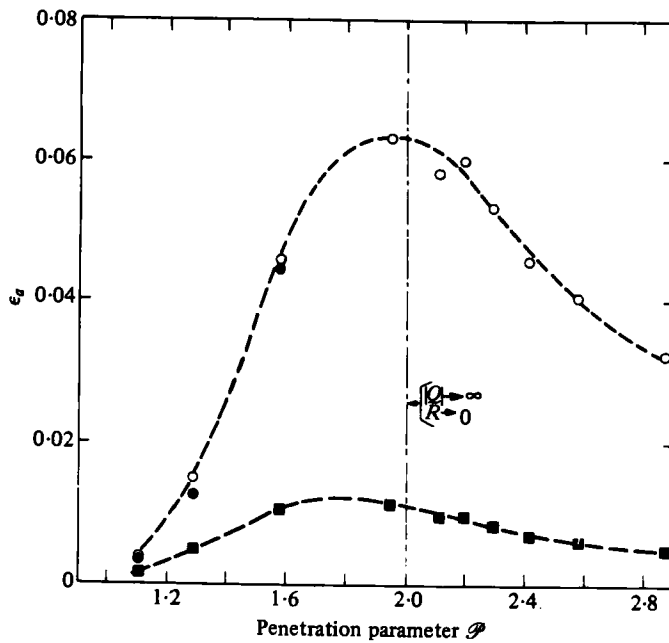

FIGURE 15. Size of the hysteresis loop at the onset of convection as a function of the penetration parameter $\mathscr{P}$. $\bullet$, $\epsilon_a = (1 - R_a/R_c)$; $\bigcirc$, $\epsilon_{au} = (1 - R_a/R_c)_u$; $\blacksquare$, $\epsilon_{aT} = (1 - \Delta T_a/\Delta T_c)$.
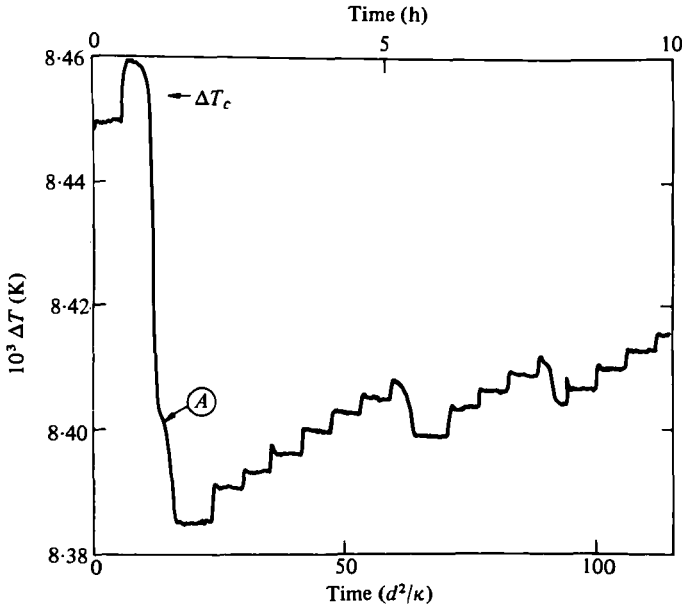
FIGURE 16. Time dependence of ΔT while the heat current q is monotonically increased in small steps. Time is measured in units of the thermal diffusion time $t_\kappa = 311$ s. $\mathscr{P} = 2\cdot20$.

region for such knees by choosing a different experimental path (decreasing q for instance). Beyond the minimum in figure 16, six small steps in q each yield a stable value of ΔT; but the seventh causes the system to enter an unstable region and results in a decay to a state of greater heat transport. After four additional steps, this decay repeats itself to yet another state. Values of Nusselt numbers as a function of $\Delta T/\Delta T_c$ corresponding to the data in figure 16 (and additional measurements for larger and smaller q) are shown in figure 17. The multistability is clearly apparent.

We believe that the existence of distinct flow states is consistent with three-dimensional convection in a laterally finite system. One expects that the lateral size of a convecting cell is approximately equal to the height l of the unstable fluid layer. This criterion determines the number n of cells which initially forms in the finite geometry. As q increases, the convection will penetrate into the upper fluid region, and the effective height of the fluid layer will increase. Thus, there will also be a tendency for the lateral size of the convecting cells to increase; but in the finite system this can occur only in discrete increments by the expulsion of one cell from the system, reducing n to $n-1$. Our interpretation thus is that successive states in figure 17 correspond to decreasing integer values of n. This interpretation suggests that the step size ΔN between successive states should decrease with increasing $\mathscr{P}$ because large $\mathscr{P}$ corresponds to small l and thus to a large initial value of n. A reduction of n to $n-1$ is then a relatively smaller change at large $\mathscr{P}$. This is indeed the case, as illustrated in figure 18, where ΔN is shown as a function of $\mathscr{P}$. The step size at constant $\mathscr{P}$ should also depend upon the aspect ratio L of the cell, and should vanish as L diverges; but we have no data on the aspect-ratio dependence.

Finally, we point out that in the case of mildly penetrative convection the data for $N(R)$ near R_c no longer agree quantitatively with the theoretical prediction for
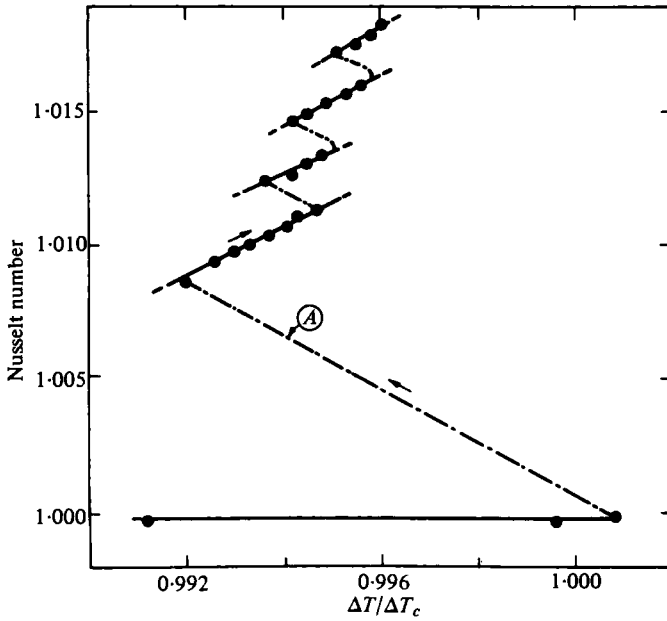
FIGURE 17. Nusselt numbers as a function of reduced temperature difference $\Delta T/\Delta T_c$ for the data of figure 16. $\mathscr{P} = 2\cdot20$. The dot-dashed lines indicate irreversible (hysteretic) transitions.
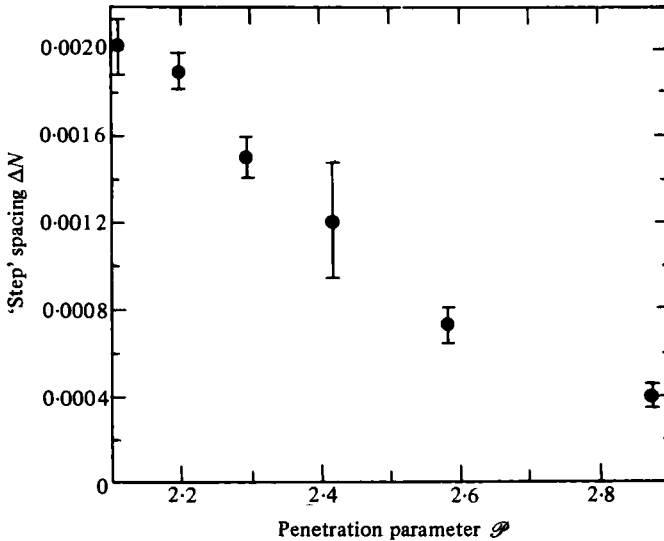

FIGURE 18. Spacing in Nusselt number between stable states as a function of penetration parameter $\mathscr{P}$.

non-OB systems as given by (7.8) of Busse (1967) if the experimental value $R_H^{(20)}$ for our near-OB case (see figure 6) is used in the theory. This is illustrated for $Q_c = -11\cdot68$ in figure 19, where the solid line corresponds to the theory, but with $R_H^{(20)}$ adjusted to fit the data in figure 6. The data points are some of those shown already in figure 8. Of course, we would not necessarily expect agreement with the theory for such large values of $|Q_c|$.
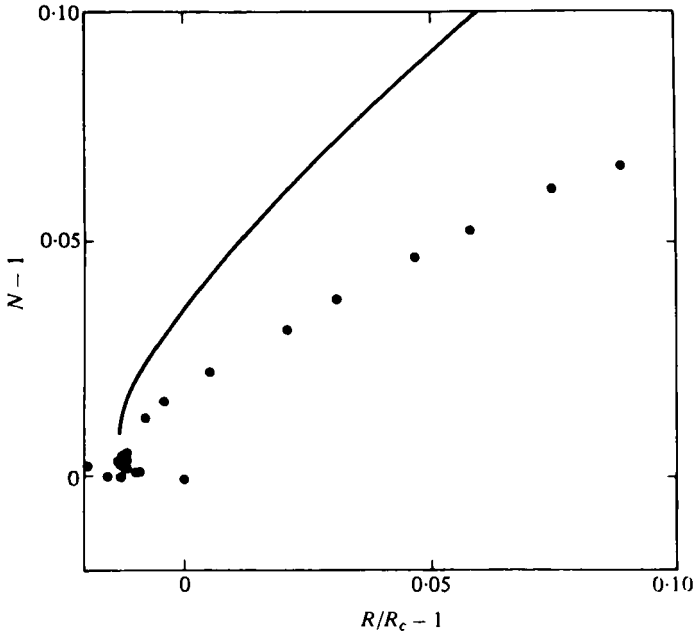
FIGURE 19. Nusselt numbers as a function of R/R_c for $Q_c = -11\cdot68$. $\mathscr{P} = 1\cdot29$. The solid line is the prediction of Busse (1967), with a parameter adjusted to fit the data in figure 6. For values of $|Q_c|$ as large as $11\cdot68$, the theory no longer agrees quantitatively with the measurements.

7. Time-dependent flow

A detailed study of time-dependent fluid-flow states was not the main objective of this work; but some observations made during the course of the measurements are worth reporting. In the nearly Boussinesq case, non-periodic time-dependent behaviour becomes obvious near $R/R_c \sim 2$ (Ahlers 1974; Ahlers & Behringer 1978; Ahlers & Walden 1980). For non-OB and penetrative convection time-dependent flow is readily observable much closer to R_c. The diagonal bars attached to some of the data points in figures 8 and 13 indicate the typical range of excursions for those particular cases.†

In figure 20 we show as solid squares the smallest values N_t of the Nusselt number N at which time-dependent behaviour has been observed, as a function of $\mathscr{P}$. We show N_t rather than the corresponding value of the Rayleigh number because of the ambiguity in the definition of R for large $\mathscr{P}$; but the data in figures 8, 9, 11 and 13 give some indication of the relation between N and R. In general, time-dependent flows were non-periodic with characteristic (mean) frequencies between $0\cdot02/t_v$ and $2/t_v$ ($t_v = 310$ sec is the vertical thermal diffusion time d^2/κ).

For $1\cdot5 \lesssim \mathscr{P} \lesssim 2$, R is less than R_c at the onset of time dependence, and no stationary fluid flow was ever observed. For larger $\mathscr{P}$, where the multistability illustrated in figures 16–18 was observed, there is a range of N for which flow is steady near the centre of the existence range of a particular flow state, but time dependent near the

† Note that in the N–R plane the excursions occur along non-vertical lines because of the constraint of constant q.
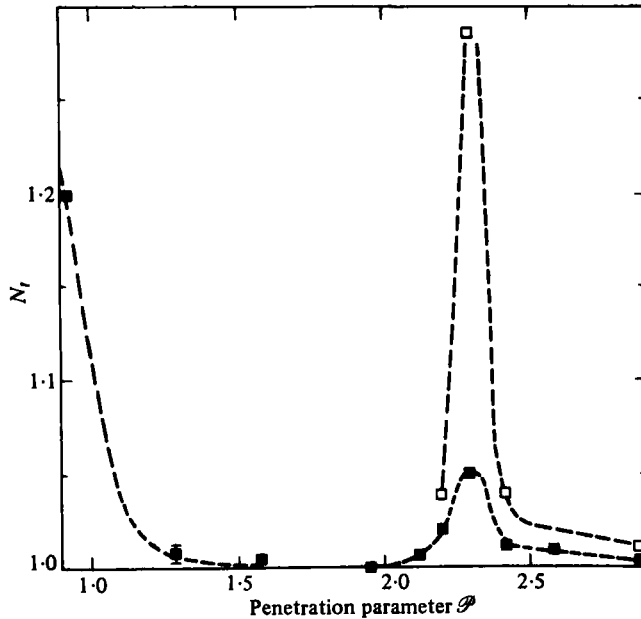
FIGURE 20. Domains of time-dependent and time-independent flow. The smallest Nusselt number N_t for which time-dependent flow was observed as a function of penetration parameter is indicated by the solid symbols. The open symbols indicate the largest values of the Nusselt number for which time-independent flow was observed in a region of multistability.

edges. We have indicated in figure 20 the highest values of N at which *steady* flow was ever observed by the open squares.

Although, in most cases, the observed time dependence was non-periodic, narrow ranges of periodic behaviour were encountered also on occasion. An example is $\mathscr{P} = 0.92$ and $1.3 \lesssim N \lesssim 1.42$, where the frequency was about $0.4/t_v$ and mildly dependent upon R. In that case, the fluid motion was non-periodic for $1.2 \lesssim N \lesssim 1.3$. The systematics of time-dependent states is clearly quite complicated for non-OB systems, and may well involve several mechanisms.

8. Summary

Studies of fluid convection in a cylindrical cell of aspect ratio $L = 4.72$ have been presented which illustrate the effects of large temperature variations of the fluid parameters. These variations were caused primarily by the temperature dependence of the thermal expansion coefficient α_p. By adjusting the temperature at the top of the cell, a wide range for the temperature dependence of α_p, including negative values near the top of the cell, could be achieved. Some of our results have been compared with the theoretical predictions by Busse (1967).

Our measurements suggest that the critical Rayleigh number R_c is slightly dependent upon the extent Q of departures from the Oberbeck–Boussinesq (OB) approximation (which assumes temperature-independent properties). But we cannot entirely rule out the possibility that this Q-dependence of R_c is attributable to systematic errors in the fluid properties. The theory for an infinite system predicts an R_c which

to first order is independent of Q. We find that, within our experimental error, the initial slope of the Nusselt number is independent of Q, consistent with the theory. The theory predicts the existence of an inverted bifurcation at R_c associated with the convective flow of hexagonal symmetry. This bifurcation was observed in all cases for which experimental resolution was expected to be sufficient to detect it. The measured width $\bar{\epsilon}_a$ of the associated hysteresis loop was about 60 % of that predicted by Busse. However, measurements of $\bar{\epsilon}_a$ were possible only in the region of penetrative convection where departures from the OB approximation are large, and where quantitative agreement with Busse's theory is least likely. In addition, our data may differ somewhat from the theory because our system is finite whereas the theory is for a laterally infinite system.

The experimentally determined values of $\bar{\epsilon}_b$ for the bifurcation from hexagonal flow to rolls were about 85 % of the theoretical values in the region of non-penetrative convection. Corresponding values of $\bar{\epsilon}_r$ for the transition from convective rolls to hexagonal flow are not resolved in the experimental data (for non-penetrative convection), but upper limits on the experimental $\bar{\epsilon}_r$ put its expected values near or below the values predicted by Busse's theory.

Several phenomena observed in penetrative convection with penetration parameter $\mathscr{P} \lesssim 3$ have not been previously observed or predicted by theory. The amplitude $\bar{\epsilon}_a$ of hysteresis at R_c grows considerably as $\mathscr{P}$ increases toward 2, then declines again at larger values of $\mathscr{P}$. For $\mathscr{P} > 2$ a series of stable states closely spaced in Nusselt number is observed near R_c. Transitions between states are suggestive of three-dimensional cells being added to or removed from the fluid volume to optimize convective transport in the presence of lateral boundaries. The spacing between states decreases with increasing $\mathscr{P}$, which should be a key in the formulation of a quantitative theory.

As the penetration parameter $\mathscr{P}$ increases beyond 1, the Nusselt number for the onset of time-dependent flow drops sharply until all flow is time-dependent at the onset of convection. However, for still greater penetration there is a region of relative stability in which the presence or absence of time dependence is influenced by the proximity of the system to a bifurcation between stable states.

REFERENCES

AHLERS, G. 1974 Low-temperature studies of the Rayleigh–Bénard instability and turbulence. *Phys. Rev. Lett.* **33**, 1185–1188.

AHLERS, G. 1975 The Rayleigh–Bénard instability at helium temperatures. In *Fluctuations, Instabilities, and Phase Transitions* (ed. T. Riste), pp. 181–193. Plenum.

AHLERS, G. 1980 Effect of departures from the Oberbeck–Boussinesq approximation on the heat transport of horizontal convecting fluid layers. *J. Fluid Mech.* **98**, 137–148.

AHLERS, G. & BEHRINGER, R. P. 1978 Evolution of turbulence from the Rayleigh–Bénard instability. *Phys. Rev. Lett.* **40**, 712–716.

AHLERS, G., CROSS, M. C., HOHENBERG, P. C. & SAFRAN, S. 1981 The amplitude equation near the convective threshold: application to time-dependent heating experiments. *J. Fluid Mech.* (to appear).

AHLERS, G. & WALDEN, R. W. 1980 Turbulence near onset of convection. *Phys. Rev. Lett.* **44**, 445–448.

AZOUNI, M. A. & NORMAND, C. 1981 Thermoconvective instability of water between 0° and 4 °C. *J. Fluid Mech.* (submitted).

BEHRINGER, R. P. & AHLERS, G. 1977 Heat transport and critical slowing down near the Rayleigh–Bénard instability in cylindrical containers. *Phys. Lett.* A **62**, 329–331.

BEHRINGER, R. P. & AHLERS, G. 1982 Heat transport and the time evolution of steady flow near the Rayleigh–Bénard instability. (To be published.)

BOGER, D. V. & WESTWATER, J. W. 1967 Effect of buoyancy on the melting and freezing process. *Trans. A.S.M.E.* C, *J. Heat Transfer* **89**, 81–89.

BROWN, S. N. & STEWARTSON, K. 1978 On finite amplitude Bénard convection in cylindrical containers. *Proc. Roy. Soc.* A **360**, 455–469.

BUSSE, F. H. 1967 The stability of finite amplitude cellular convection and its relation to an extremum principle. *J. Fluid Mech.* **30**, 625–649.

CHANDRASEKHAR, S. 1961 *Hydrodynamic and Hydromagnetic Stability.* Clarendon.

CHARLSON, G. S. & SANI, R. L. 1970 Thermoconvective instability in a bounded cylindrical fluid layer. *Int. J. Heat Mass Transfer*, **13**, 1479–1496.

DAVIS, S. H. & SEGEL, L. A. 1968 Effects of surface curvature and property variations on cellular convection. *Phys. Fluids* **11**, 470–476.

DEARDORFF, J. W., WILLIS, G. E. & LILLY, D. K. 1969 Laboratory investigation of non-steady penetrative convection. *J. Fluid Mech.* **35**, 7–31.

DUBOIS, M., BERGE, P. & WESFREID, J. 1978 Non-Boussinesq convective structures in water near 4 °C. *J. Phys.* **39**, 1253–1257.

FARHADIEH, R. & TANKIN, R. S. 1974 Interferometric study of two-dimensional Bénard convection cells. *J. Fluid Mech.* **66**, 739–752.

FURUMOTO, A. & ROOTH, C. 1961 Observations on convection in water cooled from below. *Geophysical Fluid Dynamics* 3, 14 pp. Woods Hole Oceanographic Inst.

HOARD, C., ROBERTSON, C. & ACRIVOS, A. 1970 Experiments on the cellular structure in Bénard convection. *Int. J. Heat Mass Transfer* **13**, 849–856.

KOSCHMIEDER, E. L. 1966 On convection on a uniformly heated plate. *Beitr. Phys. Atmos.* **39**, 1–11.

KOSCHMIEDER, E. L. 1969 On the wavelength of convective motions. *J. Fluid Mech.* **35**, 527–530.

KOSCHMIEDER, E. L. 1974 Bénard convection. *Adv. Chem. Phys.* **26**, 177–212.

KOSCHMIEDER, E. L. & PALLAS, S. G. 1974 Heat transfer through a shallow horizontal convecting fluid layer. *Int. J. Heat Mass Transfer* **17**, 991–1002.

KRISHNAMURTI, R. 1968 Finite amplitude convection with changing mean temperature. Part 1. Theory. Part 2. An experimental test of the theory. *J. Fluid Mech.* **33**, 445–455; 457–463.

LEGROS, J. C., LONGREE, D. & THOMAES, G. 1974 Bénard problem in water near 4 °C. *Physica* **72**, 410–414.

MARTIN, P. C. 1975 The onset of turbulence: a review of recent developments in theory and experiment. *Proc. Int. Conf. on Statistical Physics, Budapest* (ed. L. Pál & P. Szépfalusy). North-Holland.

MERKER, G. P., WAAS, P. & GRIGUBB, U. 1979 Onset of convection in a horizontal water layer with maximum density effects. *Int. J. Heat Mass Transfer* **22**, 505–515.

MOORE, D. R. & WEISS, N. O. 1973 Nonlinear penetrative convection. *J. Fluid Mech.* **61**, 553–581.

MUSMAN, S. 1968 Penetrative convection. *J. Fluid Mech.* **31**, 343–360.

MYRUP, L., GROSS, D., HOO, L. S. & GODDARD, W. 1970 Upside down convection. *Weather* **25**, 150–157.

NORMAND, C., POMEAU, Y. & VELARDE, M. G. 1977 Convective instability: a physicist's approach. *Rev. Mod. Phys.* **49**, 581–624.

PALM, E. 1960 On the tendency towards hexagonal cells in steady convection. *J. Fluid Mech.* **8**, 183–192.

PALM, E., ELLINGSEN, T. & GJEVIC, B. 1967 On the occurrence of cellular motion in Bénard convection. *J. Fluid Mech.* **30**, 651–661.

RICHTER, F. M. 1978 Experiments on the stability of convection rolls in fluids whose viscosity depends on temperature. *J. Fluid Mech.* **89**, 553–560.

ROSSBY, H. T. 1969 Bénard convection with and without rotation. *J. Fluid Mech.* **36**, 309–335.

SCHLÜTER, A., LORTZ, D. & BUSSE, F. 1965 On the stability of finite amplitude convection. *J. Fluid Mech.* **23**, 129–144.

SEGEL, L. A. 1965 The non-linear interaction of a finite number of disturbances to a layer of fluid heated from below. *J. Fluid Mech.* **21**, 359–384.

SEGEL, L. A. & STUART, J. T. 1962 On the question of the preferred mode in cellular thermal convection. *J. Fluid Mech.* **13**, 289–306.

SILVERSTON, P. L. 1958 Wärmedurchgang in Waagerechten Flüssigkeitsschichten. *Forsch. Ing.-Wes.* **24**, 29–32; 59–69.

SOMERSCALES, E. & DOUGHERTY, T. S. 1970 Observed flow patterns at the initiation of convection in a horizontal liquid layer heated from below. *J. Fluid Mech.* **42**, 755–768.

SPIEGEL, E. A. 1971 Convection in stars. I. Basic Boussinesq convection. *Ann. Rev. Astron. Astrophys.* **9**, 323–352.

SUN, Z.-S., CHI, T. & YEN, Y.-C. 1969 Thermal instability of a horizontal layer of liquid with maximum density. *A.I.Ch.E. J.* **15**, 910–915.

TANKIN, R. S. & FARHADIEH, R. 1971 Effects of thermal convection currents on formation of ice. *Int. J. Heat Mass Transfer* **14**, 953–961.

TIPPELSKIRCH, H. V. 1956 *Beitr. Phys. Atmos.* **29**, 218–233.

TOWNSEND, A. A. 1966 Internal waves produced by a convective layer. *J. Fluid Mech.* **24**, 307–319.

VERONIS, G. 1963 Penetrative convection. *Astrophysical J.* **137**, 641–663.

WALDEN, R. W. & AHLERS, G. 1979 *Bull. Am. Phys. Soc.* **24**, 1135.

WHITEHEAD, J. A. 1975 A survey of hydrodynamic instabilities. In *Fluctuations, Instabilities, and Phase Transitions* (ed. T. Riste), pp. 153–180. Plenum.

YEN, Y.-C. 1968 Onset of convection in a layer of water formed by melting ice from below. *Phys. Fluids* **11**, 1263–1270.

YEN, Y.-C. & GALEA, F. 1969 Onset of convection in a water layer formed continuously by melting ice. *Phys. Fluids* **12**, 509–516.